PHILOSOPHICAL MAGAZINE A, 1996, VOL. 74, NO. 5, 1117–1128

Nanoindentation and picoindentation measurements using a capacitive transducer system in atomic force microscopy

By BHARAT BHUSHAN, ASHOK V. KULKARNI

Computer Microtribology and Contamination Laboratory, Department of Mechanical Engineering, The Ohio State University, Columbus, Ohio 43210, USA

WAYNE BONIN and JERZY T. WYROBEK

Hysitron Inc., Minneapolis, Minnesota 55413, USA

[*Received in revised form 22 April 1996*]

ABSTRACT

An indentation system is developed to directly apply loads ranging from 1 μN to 10 mN and to make load–displacement measurements with subnanometre indentation depth capability. This system is used here in conjunction with a commercial atomic force microscope to provide *in-situ* imaging. A three-sided pyramidal (Berkovich) diamond tip has been used to obtain a load–displacement curve with residual depths of the order of 1 nm. The load–displacement data have been used to obtain indentation hardness and Young's modulus of elasticity for single-crystal silicon and GaAs. Hardness on the nanoscales is found to be higher than that on the microscale. Ceramics exhibit significant plasticity and creep on the nanoscale.

§ 1. INTRODUCTION

Mechanical properties of solid surfaces and surface thin films are of interest to tribologists as these affect the friction and wear performance of interfaces. Among the mechanical properties of interest, one or more of which can be obtained using commercial and specialized indentation hardness instruments are elastic–plastic deformation behaviour, hardness, Young's modulus of elasticity, scratch resistance, film–substrate adhesion, residual stresses, time-dependent creep and relaxation properties, fracture toughness and fatigue. Hardness implies resistance to local deformation. For hardness measurements of bulk materials and thin films, various indentation techniques are available. In order to get accurate measurements of hardness of surface films, the film thickness should be at least five times the indentation depth (Tabor 1951). Pethica, Hutchings and Oliver (1983) developed a depth-sensing instrument in which small loads can be applied so that a minimum residual indentation depth of about 20 nm can be achieved. As it becomes necessary to measure the mechanical properties of ultrathin (10 nm or less) films such as in the computer industry (Bhushan 1995, 1996a) and microsystems (Bhushan 1996b), new techniques are needed to make measurements at very shallow depths.

For nanometre-scale indentation depths, *in-situ* capabilities of imaging of the indents at extremely high magnifications is desirable. Scanning tunnelling microscopes and atomic force microscopes are ideal for *in-situ* imaging of surfaces before and after indentation. These microscopes have been used for indentation studies with

0141–8610/96 $12·00

nanometre-scale depths (Bhushan and Koinkar 1994, Bhushan, Israelachvili and Landman 1995). Atomic force microscopes are preferred because of their versatility. However, load–displacement curves cannot be obtained with high accuracy for the following reasons. First, to obtain the indentation depth, sample displacement needs to be subtracted from the tip displacement requiring subtraction of two large numbers. Second, piezoelectric transducers (PZTs) are generally used for sample motion which exhibit nonlinearity, hysteresis and creep. Nonlinearity can be corrected; however, hysteresis and creep can result in displacements of the order of the indentation depths of interest. New materials for nanoscale motions are available which minimize these effects (Hues, Draper, Lee and Colton 1994). Finally, a large lateral deflection of the cantilever beam may be required to apply high loads which changes the indentation location during loading. An indentation system with a three-plate transducer with electrostatic actuation and capacitive sensor is developed to directly apply loads ranging from 1 μN to 10 mN and to make load-displacement measurements with subnanometre indentation depth capability. When used in conjunction with an atomic force microscope, *in-situ* imaging can be obtained. The new indenter system is described in this paper. This new so-called 'nano/picoindenter' system has been used for mechanical property characterization of various materials. The results are the subject of this paper.

§ 2. Nano/picoindenter with three-plate transducer with electrostatic actuation and capacitive sensor

An overall schematic diagram of the new indentation system (Hysitron Inc.) using an atomic force microscope (such as Nanoscope III, Digital Instruments) as a platform is shown in fig. 1 (*a*). The indentation system consists of a new three-plate transducer with electrostatic actuation hardware used for direct application of normal load and a capacitive sensor used for measurement of vertical displacement (fig. 1 (*b*)). The atomic force microscope head is replaced with this transducer, and the sample is mounted on the PZT scanner. The transducer has a three (Be–Cu) plate capacitive structure which provides a high sensitivity, a large dynamic range and a linear output signal with respect to load or displacement. The tip is connected to the centre plate which is spring mounted to the housing. Four springs are mounted on the top and another four are mounted at the bottom with a total stiffness of 100 N m^{-1}. Vertical displacement of the tip (indentation depth) is measured by measuring the displacement of the centre electrode relative to the two outer electrodes using the capacitance technique. During measurements, the sample remains stationary. The load is applied by an electrostatic force generated between the centre (pick-up) electrode and drive plate (upper or lower) when a voltage is applied to the drive plate. The applied load is proportional to square of the voltage. The load resolution is 100 nN or better and the displacement resolution is 0·1 nm. At present, a load range of 1 μN–10 mN can be used. Loading rates can be varied changing the load–unload period from 180 to 950 s. The atomic force microscope functions as a platform for the indenter system and also provides *in-situ* imaging before and after indentation with a lateral resolution of about 10 nm and a vertical resolution of about 0·2 nm. Load–displacement data during loading and unloading are obtained.

A three-sided pyramidal (Berkovich) tip with a tip radius of about 0·1 μm and made of diamond has been used for the measurements (Berkovich 1951, Bhushan 1995), although diamond tips with sharper included angles (60–90°) and tip radii (30–60 nm) are used for shallower indentations (of the order of 1 nm). A titanium

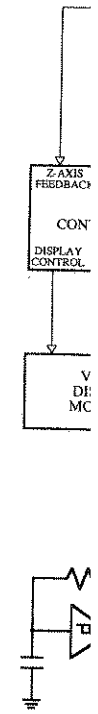

Schematic di
electr
assen

Fig. 1

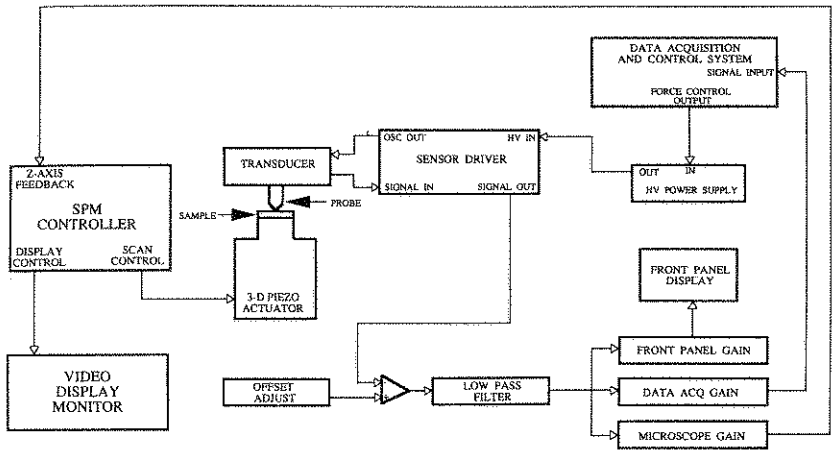

Schematic diagrams of (*a*) the nano/picoindenter system, (*b*) the three-plate transducer with electrostatic actuation hardware and capacitance sensor and (*c*) tip–holder mount assembly.

shank brazed to the diamond tip is glued to a glass-reinforced plastic (Ryton) holder which in turn is screwed into the centre plate (fig. 1 (*c*)). The exact shape of the indenter tip needs to be measured to obtain an accurate projected contact area–depth relationship and for the determination of hardness and Young's modulus of elasticity. Tip-shape calibration is carried out so that the indentation depth can be related to the projected contact area. Hardness data are also obtained from direct imaging of the indentation marks. For surfaces with rms roughness of the order of the indentation depth, the original (unindented) profile is subtracted from the indented profile (Bhushan and Koinkar 1994). Surface imaging allows one to quantify the piling up of ductile material around the indenter to obtain correct values of the contact area. However, it is difficult to identify the boundary of the indentation mark which makes the direct measurement of contact area somewhat inaccurate. In the hardness data presented in this paper, pile-up effects are neglected. For scratch and wear studies, the PZT scanner can be used to translate the sample.

2.1. *Electrostatic actuation*

An electrostatic force is generated between the centre (pick-up) electrode and drive plate when a voltage is applied to the drive plate (see fig. 1 (*b*)). This force is given by a simple analytical function of bias voltage, plate area and plate spacing:

$$F = \tfrac{1}{2}\epsilon A E^2, \tag{1}$$

where ϵ is the dielectric constant ($8{\cdot}854 \times 10^{-12}\,\mathrm{F\,m^{-1}}$, in air or vacuum), A is the plate area ($5{\cdot}8 \times 10^{-5}\,\mathrm{m^2}$ for the present design) and E is the electric field in volts per metre. The drive plates 1 and 2 are fixed, so that $d_1 + d_2$ is a constant (about 250μm). The pick-up electrode can move up and down in the space between the two drive plates. The electrostatic voltage is normally applied to only one drive plate at a time, and the pick-up electrode is attracted towards that plate.

For a given pick-up electrode position, the pick-up to the drive plate spacing d is a constant, and the electric field strength is

$$E = \frac{V}{d}, \tag{2}$$

where V is the applied voltage and d is the spacing in metres. Replacing E in eqn. (1) with V/d gives

$$F = \tfrac{1}{2}\epsilon A\left(\frac{V}{d}\right)^2 \tag{3}$$

$$= k_e V^2, \tag{4}$$

where k_e is an electrostatic force constant. Equation (4) is used to determine the tip-to-sample force during indentation. (The capacitance signal provides the depth–displacement data.)

Two factors reduce the accuracy of the force measurement of the method just described. Both factors arise because the spacing d is not exactly constant during the indentation. As the tip penetrates into the sample during the indentation, d is reduced by the amount of penetration. This increases the electric field strength for a given voltage, thereby increasing the amount of electrostatically generated force. This effect is small, about 2% or less for indentations of less than 1 μm depth. The effect does increase rapidly above 1 μm, reaching a factor of two at 30 μm (for 100 μm

original spacing). Note that the actual force generated is equal to the value from eqn. (4) multiplied by the increase in force generated corresponding to the deflection and original electrode spacing.

The other factor affecting accuracy is due to the spring constant of the suspension that supports the pick-up electrode. The suspension springs support part of the electrostatically generated force. The actual force supported by the sample is the total generated force minus the deflection times the support spring constant. This spring constant is about $100\,\mu N\,\mu m.^{-1}$ This effect is significant at all loads and displacements, except with very hard samples where the tip-to-sample stiffness is much greater than the suspension spring constant. The shape of the unloading curve is affected more than that of the loading curve since, as the force returns toward zero, the permanent indentation depth from the indentation will leave the tip 'hanging' in the air above the indent. This results in only part of the unloading curve representing the sample properties, and the final section representings the transducer spring constant, with the point of return to zero force not being properly represented on the curve. For very hard materials such as GaAs, silicon and Al_2O_3, this can be compensated for by introducing a small preload force before performing the indent. With these materials, a preload of 5% or less of the peak force will keep the tip in contact with the sample at the end of the indentation cycle when the electrostatic force returns to zero. The preload is applied by deflecting the support springs in the transducer by moving the z-axis piezo actuator holding the sample. For softer materials, the preload required to maintain contact after indentation is excessive, being over 20% of the peak load for the softer materials such as aluminium.

The current data acquisition software already determines the displacement from the sensor output; so the actual force applied to the sample can be determined as follows. For small displacements, less than 1 μm, assume that eqn. (4) gives the electrostatically generated force

$$F_g = k_e V^2. \tag{5}$$

Then the tip-to-sample applied force is

$$F_a = F_g - k_s\,\Delta d, \tag{6}$$

where k_s is the transducer spring constant equal to approximately $100\,\mu N\,\mu m^{-1}$, and Δd is the displacement from the original pre-indent position. For large displacements, over 1 μm, the effect of changing the plate spacing on the actual electric field strength must be included. Starting with eqn. (3), let d be the plate spacing at the original calibrated position, and let the actual spacing be represented by $d - \Delta d$. Replacing d in eqn. (3) by $d - \Delta d$ gives

$$F_g = \tfrac{1}{2}\frac{\epsilon A V^2}{(d - \Delta d)^2}. \tag{7}$$

Substituting $k_e = \frac{1}{2}\epsilon A/d^2$, we get

$$F_g = k_e V^2 \left(\frac{d}{d - \Delta d}\right)^2. \tag{8}$$

This shows that the true electrostatic force is equal to the simplified value now being used, multiplied by the correction factor $[d/(d-\Delta d)]^2$. As in the case of small displacements, the actual force applied to the sample is

$$F_a = F_g - k_s\,\Delta d = k_e V^2 \left(\frac{d}{d-\Delta d}\right)^2 - k_s\,\Delta d. \tag{9}$$

2.2. *Tip shape calibration and calculation procedure*

Tip shape calibration is carried out based on a method by Oliver and Pharr (1992). Indentations were made in single-crystal aluminium (100) and single-crystal GaAs(100). Because of its low hardness, aluminium produces deeper indents than GaAs does for the same indenter load. However, very shallow indents can be made in GaAs at higher loads, resulting in improved load resolution. In the present study, the contact depth defined as the depth of indenter in contact with the sample under load, ranged from 5 to 75 nm. To obtain tip shape calibration in this displacement range, GaAs was a suitable material. On the assumption that the modulus of elasticity of GaAs is constant and is equal to 99·5 Gpa (Anonymous 1990), an area function, relating projected contact area A to contact depth h_c, is obtained by fitting the data through an eighth-order polynomial (Bhushan 1995). The area function curve for the indenter used here is shown in fig. 2. The function is given as

$$A = 24{\cdot}5h_c^2 + 793h_c + 4238h_c^{1/2} + 332h_c^{1/4} + 0{\cdot}059h_c^{1/8} + 0{\cdot}069h_c^{1/16} + 8{\cdot}68h_c^{1/32} + 35{\cdot}4h_c^{1/64} + 36{\cdot}9h_c^{1/128}.$$

A and h_c are in square nanometres and in nanometres respectively. The first term describes the perfect shape of the indenter; the others describe deviations from Berkovich geometry due to blunting of the tip. This area function is used to get the projected contact area and the indentation hardness is given by normal load divided by the contact area. The hardness is calculated only for the peak load. Young's modulus of elasticity is obtained from the slope of the unloading curve at the maximum load (Bhushan 1995). The unloading curve is generally nonlinear at

Fig. 2

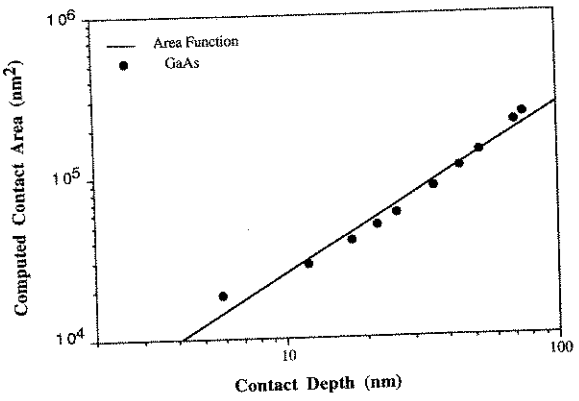

Computed contact area as a function of contact depth.

the maximum load; therefore the measured slope depends on how many of the data are used in the fit. To minimize this error, one third of the unloading data are fitted with a simple power law relation. The initial unloading slope is found analytically by differentiating this expression and evaluating the derivative at the maximum load and maximum depth. In this analysis, Young's modulus of elasticity and Poisson's ratio for diamond were taken as 1140 Gpa and 0·07 respectively. Poisson's ratio for silicon was taken as 0·28.

2.3. *Operation procedure*

The tip is lowered towards the sample so that it is positioned close (ideally less than 100 μm) to the sample. The scan size and scan speed are selected. The tip is then engaged to the sample by using the stepper motor with a set point of about 1 nA (about 1 μN load). The sample is imaged before indentation. For an indentation experiment, the feedback is set to zero to disable the scanner and a set point for an appropriate peak load and indentation rate are selected. For all experiments except for loading rate, the load–unload duration was 180 s. The indentation experiment is carried out and post-indent image is captured.

§ 3. Results and discussion

A load–displacement curve for a single-crystal silicon (100) at peak loads of 500 μN is shown in fig. 3 (*a*). These data are compared with those obtained using

Fig. 3

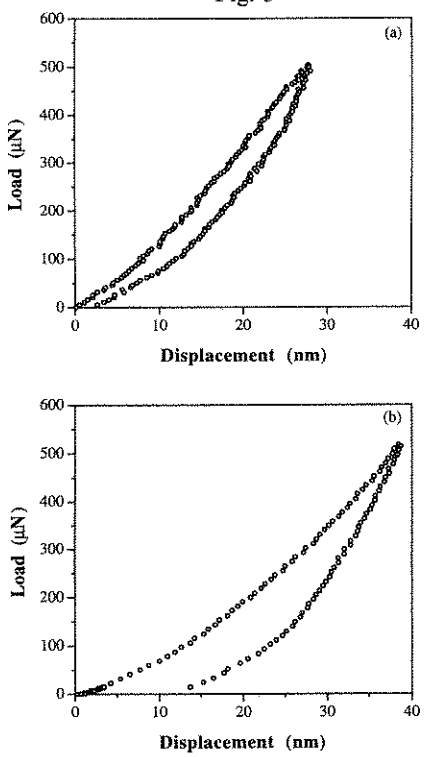

Load–displacement curves for single-crystal silicon obtained using (*a*) the new indentation system and (*b*) a commercial Nanoindenter II.

a commercial Nanoindenter II (fig. 3 (*b*)). Data obtained from both instruments have similar trends. Slight differences result from the shape differences in the tips used in the two instruments. Figure 4 (*a*) shows the load–displacement curves at different peak loads for single-crystal silicon and GaAs. Typical atomic force microscopy (AFM) images of indents made on single-crystal GaAs and silicon are given in fig. 5. Load–displacement data at residual depths as low as 2 nm can be obtained. Note

Fig. 4

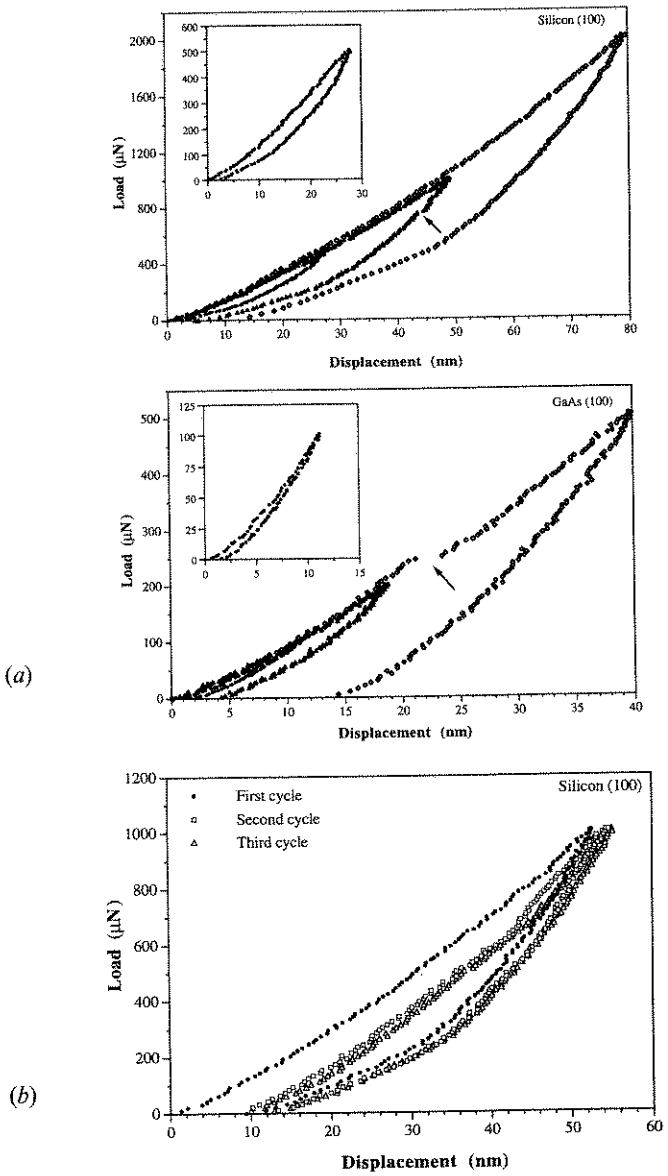

Load–displacement curves (*a*) at various peak loads for single-crystal silicon and GaAs, and (*b*) during repeated loading–unloading cycles.

AFM ima

Fig. 5

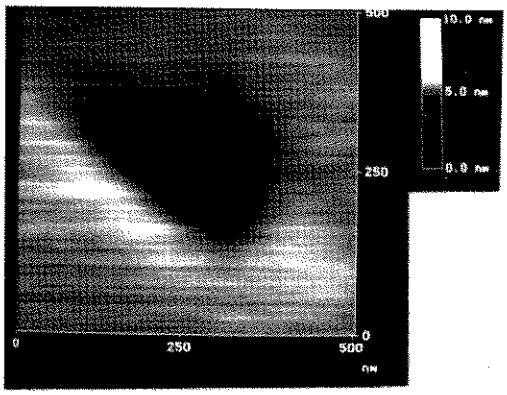

GaAs(100), 500 μN

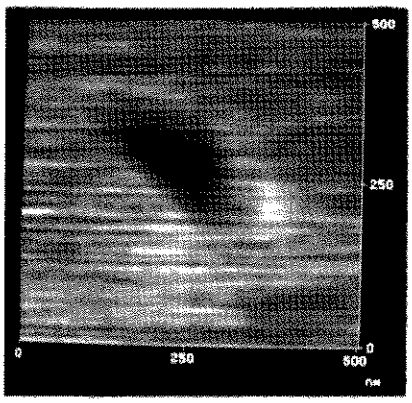

Silicon(100), 500 μN

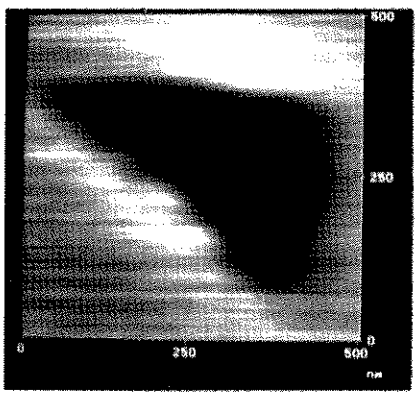

Silicon(100), 2000 μN

AFM images of single-crystal GaAs and silicon surfaces after performing indentation at various peak loads.

that load–displacement curves during unloading are not linear; each curve is slightly concave upwards over its entire range. Further, note that the loading and unloading curves are not smooth but exhibit sharp discontinuities particularly at high loads (shown by arrows in fig. 4 (*a*)). Discontinuities in the loading part of the curve results from slip. Pharr, Oliver and Clarke (1990) and Pharr (1992) reported the evidence of discontinuities in the unloading curves and hypothesized that a sharp discontinuity is due to formation of a lateral crack which forms at the base of median crack, causing the surface of the specimen to be thrust upwards.

Figure 4 (*b*) shows the load–displacement curves during three loading and unloading cycles for single-crystal silicon. The unloading and reloading curves show a large 'hysteresis' which shows no sign of degeneration through 3 cycles of deformation and the peak load displacements shift to higher values in successive loading–unloading cycles. Pharr, Oliver and Clarke (1989), Pharr *et al.* (1990), Page, Oliver and McHargue (1992) and Pharr (1992) have also observed hysteresis behaviour in silicon at similar loads using a nanoindenter. The fact that the curves are highly hysteretic implies that deformation is not entirely elastic. Pharr (1992) concluded that large hysteresis is due to a pressure-induced phase transformation from its normal diamond cubic form to a β-tin metal phase (Bhushan 1995).

The table summarizes the hardness and Young's modulus of elasticity data at various depths for single-crystal silicon. Comparison of nanohardness values with that of bulk hardness shows that nanohardness of silicon is higher than its bulk hardness. Figure 6 shows the plot of hardness and Young's modulus of elasticity as functions of residual depth. Note that hardness increases with a decrease in the residual depth. Similar results on single-crystal silicon have been reported by Pethica *et al.* (1983) and Page *et al.* (1992) based on nanoindentation data and by Bhushan and Koinkar (1994) based on AFM data. Gane and Cox (1970) reported similar results on gold based on microindenter data. This increase in hardness with a decrease in indentation depth can be rationalized on the basis that, as the volume of deformed material increases, there is a higher probability of encountering material defects (Bhushan *et al.* 1995). The increase in hardness also could be due to surface-localized cold work resulting from polishing.

Comparison of nanohardness of single-crystal silicon (100) as a function of normal load, obtained by area function curve and *in-situ* imaging. Young's modulus of elasticity data on nanoscale are also listed.

Normal load (μN)	Residual depth (nm)	Contact depth (nm)	Hardness† (GPa) based on the following		Young's modulus of elasticity† (GPa)
			In-situ imaging	Area function curve	
500	2·8	17·4	18·5	13·0	160
700	7·0	25·4	17·2	12·7	141
1000	8·5	32·2	17·0	13·2	143
1200	9·5	37·0	16·5	13·4	141
2000	15·0	55·3	14·9	13·1	141

†Bulk values of hardness and Young's modulus of elasticity are 9–10 GPa and 130 GPa respectively.

Fig. 6

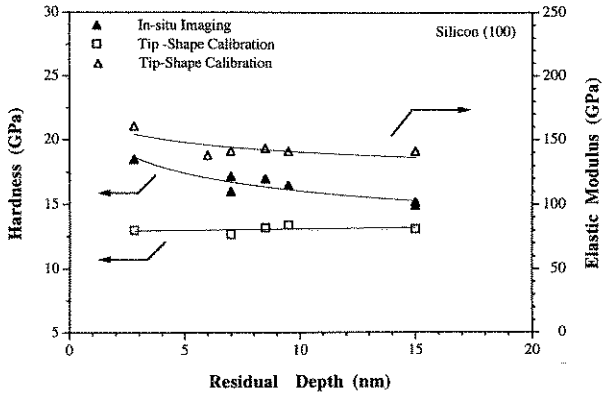

Hardness and Young's modulus of elasticity as functions of residual indentation depth for single-crystal silicon.

Most materials including ceramic and even diamond are known to creep at temperatures well below half their melting points, even at room temperature (Bhushan 1995). Indentation creep and strain rate sensitivity experiments were conducted on single-crystal silicon. Figure 7 shows the load–displacement curves for various peak loads held at 180 s. To demonstrate the creep effects, the load–displacement curves for a 500 μN peak load held at 0 and 30 s are also shown as an inset. Note that significant creep occurs at room temperature. Nanoindenter experiments conducted by Li, Henshall, Hooper and Easterling (1991) exhibited significant creep only at high temperatures (greater than or equal to 0·25 times the melting point of silicon). The mechanism of dislocation glide plasticity is believed to dominate the indentation creep process. To study strain-rate sensitivity of silicon, experiments were conducted at two different (constant) rates of loading (fig. 8). Note that a change in the loading rate of factor of about five results in a change in the load–

Fig. 7

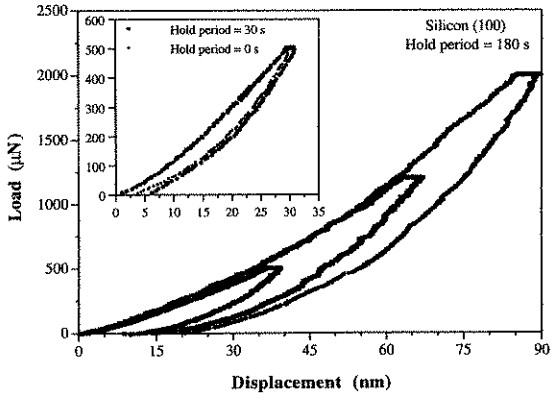

Creep behaviour of single-crystal silicon.

Fig. 8

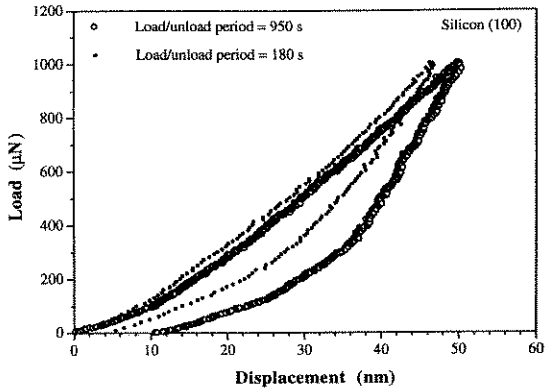

Load–displacement data for two load–unload periods.

displacement data. Strain-rate sensitivity to single-crystal aluminium (111) has been reported by LaFontaine, Yost, Black and Li (1990).

§ 4. Conclusions

An indentation system used in conjunction with an atomic force microscope provides combined capability of mechanical testing on nanoscales to picoscales and high-resolution *in-situ* imaging in a single system. This instrument has been successfully used to study load–displacement behaviour, hardness, Young's modulus of elasticity, creep and strain-rate sensitivity of single-crystal silicon and GaAs.

References

Anonymous, 1990, *Properties of Gallium Arsenide*, second edition, INSPEC, EMIS Data Reviews, Series No. 2 (Stevenage, Herts: INSPEC).

Berkovich, E. S., 1951, *Ind. Diamond Rev.*, **11**, 129.

Bhushan, B., 1995, *Handbook of Micro/Nanotribology* (Boca Raton, Florida: CRC Press); 1996a, *Tribology and Mechanics of Magnetic Storage Devices*, second edition (New York: Springer); 1996b, *Proceedings of the Ninth IEEE Annual International Workshop on Micro Electro Mechanical Systems* (New York: IEEE), pp. 91–98.

Bhushan, B., and Koinkar, V. N., 1994, *Appl. Phys. Lett.*, **64**, 1653.

Bhushan, B., Israelachvili, J. N., and Landman, U., 1995, *Nature*, **374**, 607.

Gane, N., and Cox, J. M., 1970, *Phil. Mag.*, **22**, 881.

Hues, S. M., Draper, C. F., Lee, K. P., and Colton, R. J., 1994, *Rev. scient. Instrum.*, **65**, 1561.

LaFontaine, W. R., Yost, B., Black, R. D., and Li, C. Y., 1990, *J. Mater. Res.*, **5**, 2100.

Li, W. B., Henshall, J. L., Hooper, R. M., and Easterling, K. E., 1991, *Acta metall. mater.*, **39**, 3099.

Oliver, W. C., and Pharr, G. M., 1992, *J. Mater. Res.*, **7**, 1564.

Page, T. F., Oliver, W. C., and McHargue, C. J., 1992, *J. Mater. Res.*, **7**, 450.

Pethica, J. N., Hutchings, R., and Oliver, W. C., 1983, *Phil. Mag.* A, **48**, 598.

Pharr, G. M., 1992, *Thin Films: Stresses and Mechanical Properties III*, Materials Research Society Symposium Proceedings, Vol. 239, edited by W. D. Nix, J. C. Braveman, E. Arzt and L. B. Freund (Pittsburgh, Pennsylvania: Materials Research Society), pp. 301–312.

Pharr, G. M., Oliver, W. C., and Clarke, D. R., 1989, *Scripta metall.*, **23**, 1949; 1990, *J. electron. Mater.*, **19**, 881.

Tabor, D., 1951, *The Hardness of Metals* (Oxford: Clarendon).